RSC Advances

PAPER

View Article Online
View Journal | View Issue

Cite this: *RSC Adv.*, 2021, **11**, 37544

Electrochemical sensor formed from poly(3,4-ethylenedioxyselenophene) and nitrogen-doped graphene composite for dopamine detection†

Aygul Kadir,[ab] Ruxangul Jamal,[b] Tursun Abdiryim, *[a] Nurbiya Sawut,[a] Yuzhu Che,[a] Zulpikar Helil[a] and Hujun Zhang[a]

In this study, an electrochemical sensor for dopamine (DA) detection has been developed by a composite of poly(3,4-ethylenedioxyselenophene) (PEDOS) and nitrogen-doped graphene (PEDOS/N-Gr) using an *in situ* polymerization method. Its structure and properties were then compared with those of the composites of poly(3,4-ethylenedioxythiophene) (PEDOT)/nitrogen-doped graphene (PEDOT/N-Gr), which were prepared by the same methods. FT-IR, Raman, UV-vis, XPS, mapping and SEM investigated the structure and morphology of these composites. These revealed that PEDOS/N-Gr had a higher conjugation degree than PEDOT/N-Gr. The synergetic effect between PEDOS and N-Gr was beneficial for the formation of a homogenous surface coating. The cyclic voltammetry (CV) and differential pulse voltammetry (DPV) methods were conducted for electrochemical detection of DA. Compared with PEDOT/N-Gr, the PEDOS/N-Gr displayed an enhanced sensitivity and electrocatalytic performance for DA detection with linear ranges of 0.008–80 μM (PEDOT/N-Gr: 0.04–70 μM) and limits of detection (LOD) of 0.0066 μM (S/N = 3) (PEDOT/N-Gr: 0.018 μM (S/N = 3)).

Received 19th September 2021
Accepted 5th November 2021

DOI: 10.1039/d1ra07024j

rsc.li/rsc-advances

Introduction

DA is an indispensable component of the neural system. It plays a vital role in physiological functions,[1,2] and acts as a natural neurotransmitter that helps control the central nervous system and regulate normal cardiovascular, renal and hormonal functions.[3,4] Generally, DA detection is performed by various methods, such as ultraviolet-visible spectroscopy,[5] capillary electrophoresis,[6,7] chemiluminescence[8,9] and spectrometry,[10] but most of the above techniques require complicated processes, professional training, and high-cost and specialized instruments. In contrast, the electrochemical sensing of DA can overcome these disadvantages by adopting promising electrode materials, such as carbon-based nanomaterials,[2,11] metal nanoparticles,[12,13] polymeric materials[14,15] and nanocomposites.[16,17] More and more studies have shown that common electrode materials, for example, conducting polymers,[18,19] graphene,[20] carbon nanotubes[21] and some metal oxides[22] have been applied for electrochemical sensing fields and reported. Among them, graphene-based materials have been extensively explored as promising objects which exhibit large specific surface area, high electronic transport behavior, excellent electrocatalytic property and good stability.[23,24] However, stacking of graphene-based materials usually decreases the electrochemical sensor's performance. Therefore, in the past few years, nitrogen-doped graphene (N-Gr) has gradually become one of the research hotspots in the field of electrocatalysis. As it is known that the pyridine-N, pyrrole-N and graphitic-N structures are formed due to the introduction of nitrogen heteroatoms into the planar sp^2 carbon network of graphene. This is beneficial to enhance the charge distribution on the graphene surface and increase the density of free carrier to improve its electrocatalytic activity.[25] Thereby, N-Gr is considered as a preferred electrode material for electrochemical sensors.[26–28]

In recent years, conducting polymers/graphene composites have been widely studied for the effective electrochemical sensors. For example, Manivel *et al.* prepared polyaniline/graphene oxide nanocomposite and applied it for sensitive and selective detection of DA.[29] He's group fabricated a PEDOT/N-G composite sensor for DA detection with high sensitivity, and they found that PEDOT component can improve the hybrids' conductivity and decrease N-G's stacking.[30] PEDOT exhibits good conductivity, easy processability and thermal stability, considered the essential and typical polymer for the construction of electrochemical sensors.[31,32] PEDOS is similar to PEDOT, which can avoid the formation of α, β coupling and

[a]*Key Laboratory of Energy Materials Chemistry, Ministry of Education, Key Laboratory of Advanced Functional Materials, Institute of Applied Chemistry, College of Chemistry, Xinjiang University, Urumqi, 830046, Xinjiang, PR China. E-mail: tursunabdir@sina.com.cn*

[b]*Key Laboratory of Petroleum and Gas Fine Chemicals, Ministry of Education, College of Chemical Engineering, Xinjiang University, Urumqi, 830046, Xinjiang, PR China. E-mail: jruxangul@sina.com*

† Electronic supplementary information (ESI) available. See DOI: 10.1039/d1ra07024j

β coupling products during polymerization.[33–35] PEDOS also has better structural regularity, lower oxidation potential, and better environmental stability.[36,37] PEDOS is more easily polarized and shows a lower band gap than PEDOT, which enabled it to display great electrocatalytic performance with higher electron transfer ability and conductivity.[38] As far as we know, there are few reports for the application of the PEDOS in the electrocatalytic sensors. Considering this, we developed a novel π-conjugated polymer for the electrochemical detection of DA.[39]

Herein, we reported the preparation of PEDOS and nitrogen-doped graphene (PEDOS/N-Gr) composite as an electrocatalytic sensor for detection of DA. The electrochemical properties of PEDOS/N-Gr for DA detection were examined by CV and DPV methods, and its structure and electrochemical performance were then compared with the composite of PEDOT/N-Gr which was obtained from the same method. As PEDOS has excellent interchain charge transfer ability and lower oxidation-reduction property, its monomers are easy to conjugate with N-Gr by producing the π–π stacking, which is beneficial for the uniform coating of PEDOS on the N-Gr surface and interacting with DA by hydrogen bond and π–π tacking. Consequently, all these factors can enhance sensitivity and selectivity of the composite materials to detect DA. The potential application of the composites as electrode materials for electrochemical sensing of DA was systematically evaluated.

Experimental section

Chemicals and reagents

Butan-2,3-dione, trimethyl orthoformate, sulfonyl chloride, *p*-toluene sulfonic acid (*p*-TSA) and ethylene glycol as raw materials synthesize for monomer and anhydrous ferric chloride ($FeCl_3$) as an oxidant were brought from J&K Scientific Ltd. Cetyltrimethylammonium bromide (CTAB) as a surfactant. Chloroform ($CHCl_3$), methanol and toluene as solvents and were brought from Aladdin. Monosodium orthophosphate (NaH_2PO_4), and disodium hydrogen phosphate (Na_2HPO_4) were brought from Macklin as buffering agents. Nitrogen-doped graphene (N 3.0–5.0 wt%) was brought from XF NANO, Inc.

Synthesis of EDOS

2,3-Dimethoxy-1,3-butadiene, 3,4-dimethoxyselenophene, and 3,4-ethylenedioxyselenophene (EDOS) were prepared according to a previously reported method[34,40] and the detailed information was described in ESI.†

Synthesis of PEDOS

Anhydrous ferric chloride ($FeCl_3$) (0.172 g) was dispersed in 10 ml $CHCl_3$, and was then added into a round-bottom flask and sonicated for 15 minutes. EDOS monomer was (1 ml, 0.026 mmol) dissolved in 5 ml $CHCl_3$ and slowly added into the above mixture under ultrasound guidance. The suspension was stirred at the room temperature. Finally, the mixture was purified with chloroform, ethanol, distilled-water, and PEDOS was obtained as black powder by freeze-drying.

Preparation of PEDOS/N-Gr composite

PEDOT/N-Gr and PEDOS/N-Gr were fabricated *via* a chemical oxidation polymerization. A typical preparation procedure was as follows: 0.160 g of CTAB and 0.025 g of N-Gr were added in to 20 ml $CHCl_3$, and then 0.050 g EDOS monomer was slowly added to the above system, followed by ultrasonic dispersion for 10 minutes. Finally, 0.172 g of anhydrous $FeCl_3$ was ultrasonically dispersed in the $CHCl_3$, and was added into the above mixture and stirred at ambient temperature for one day. Finally, the mixture was purified with chloroform, ethanol, distilled-water, and PEDOS/N-Gr was obtained by freeze-drying. The PEDOT/N-Gr composite was prepared by a similar process.

Structure characterization

The FT-IR of the composites was obtained by BRUKER-QEUINOX-55 FTIR spectrometer using KBr pellets. Raman spectrum were recorded with a Bruker Vertex 70 FT Infrared Spectrometer, and the range of 300–4000 cm^{-1} with λ_{ex} = 785 nm. UV-vis spectrum of composites was collected on a UV-vis spectrophotometer (UV2550 Unico, Japan). The morphology of samples was analysed by scanning electron microscopy (SEM, SO8010, Japan). X-ray photoelectron spectroscopy (XPS) was recorded with an ESCALAB 250Xi spectrometer.

Electrochemical measurements

The electrocatalytic performance of all samples was investigated *via* the CHI660E (Chen Hua Instruments, Shanghai, China) electrochemical workstation. A three-electrode system was used to study the electrochemical activity of the samples. Pt electrode, composite modified electrode (glassy carbon electrode (GCE), diameter = 4 mm) and calomel electrode were utilized as counter electrode, working electrode and reference electrode, respectively. The composite modified GCE was prepared by all the samples suspension dropped on the cleansed GCE. The CV of the composites was recorded in mixture of 5 mM $[Fe(CN)_6]^{3-/4-}$ and 0.1 M KCl with 50 mV s^{-1} scanning rate. DA was detected by the DPV method in 0.1 M PBS buffer solution (pH = 7). Different pH values of phosphate-buffered saline (PBS) solutions were obtained by 0.1 M Na_2HPO_4 and 0.1 M NaH_2PO_4.

Results and discussion

Fig. 1(a) illustrates the FT-IR of the EDOS and PEDOS. The peaks of the PEDOS are broadened significantly compared with the EDOS, owing to its complex structure and broad chain length distribution. The peak at 3112 cm^{-1} is assigned to the C–H stretching from the 2,5-position of the selenophene ring in the EDOS, while PEDOS had no this peak.[41] This result indicated that the PEDOS is successfully obtained by *in situ* polymerization. The possible mechanism for the formation of PEDOS is as follows (Scheme 1). EDOS monomer was firstly oxidized by the $FeCl_3$ to lose one electron on the β-C position, leading to the formation of the β-C positive ion, and then the new C–C sigma bond is formed by contacting with two radical positive ions at the two EDOS. After that, a pair of electrons on the α-C either bound with the β-C positive ions to form another double bond

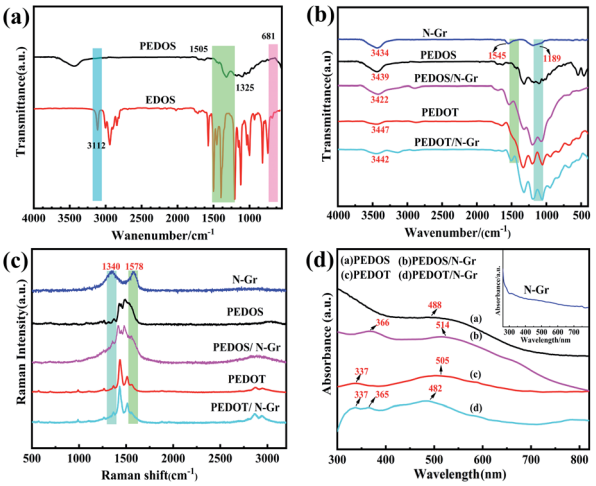

Fig. 1 (a) FT-IR spectrum of EDOS and PEDOS (b) FT-IR spectrum of N-Gr, PEDOS, PEDOS/N-Gr, PEDOT and PEDOT/N-Gr (c) Raman spectrum of N-Gr, PEDOS, PEDOS/N-Gr, PEDOT and PEDOT/N-Gr (d) UV-vis spectrum of N-Gr, PEDOS, PEDOS/N-Gr, PEDOT and PEDOT/N-Gr.

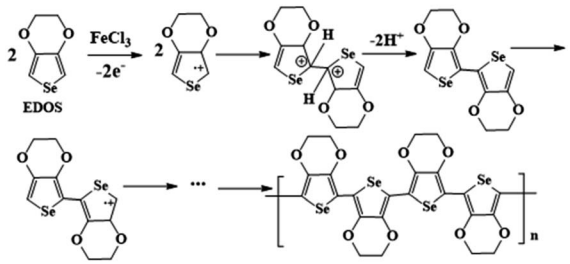

Scheme 1 The possible mechanism for oxidative polymerization of PEDOS.

or rearranged. In order to make the compound to hold the lowest energy as possible, one of the electrons on the α-C will be distributed to the β-C, while β-C is no longer charged, and α-C brings gives one electron to each of β-C, forming an additional π bond.[42] Fig. 1(b) illustrates the FTIR of the N-Gr, PEDOS, PEDOT, PEDOS/N-Gr and PEDOT/N-Gr. As shown in Fig. 1(b), the spectrum of PEDOS containing the bands at 951, 840, and 688 cm^{-1} can be contributed to the stretching vibration of C–Se. The vibration bands at 1318 and 1505 cm^{-1} correspond to the C–C inter-ring stretching and the C=C asymmetric stretching. The bands at 1178, 1103 and 1047 cm^{-1} are assigned to the C–O–C in the ethylenedioxy parts.[41,43]

For N-Gr, the band around at 3434 cm^{-1} is usually followed to the N–H stretching vibrations. The other main two bands at 1189 and 1545 cm^{-1} are attributed to the stretching vibrations of the C–N and C=N, further implying the strong binding between graphene matrix and nitrogen atoms.[44] For PEDOS/N-Gr composite, the bands at 687, 966, 1057, 1190, 1346, 1380 and 3432 cm^{-1} confirm the successful formation of PEDOS, while the bands at 1532 cm^{-1} is associated with the N-Gr. After combined with N-Gr, a comparison reveals the intensity of peak at 1178 cm^{-1} in PEDOS move to 1197 cm^{-1}, consequently overlapping the bands at 1189 cm^{-1} and 1178 cm^{-1}, which belongs to N-Gr and PEDOS, respectively. All these results indicate that N-Gr is incorporated into PEDOS. For PEDOT/N-Gr, the vibration bands at 685, 838, 921, 1059, 1193, 1320, 1513 and 3449 cm^{-1} are assigned to the PEDOT, while the characteristic band at 1513 cm^{-1} is originated from N-Gr. After combined with N-Gr, a comparison also reveals that the main three peaks at 3434, 1545 and 1189 cm^{-1} are overlapped with that of PEDOT at the same wavenumber, indicating the successful incorporation of N-Gr with PEDOT.

Fig. 1(c) represents the Raman spectrum of N-Gr, PEDOS, PEDOT, PEDOS/N-Gr and PEDOT/N-Gr. As shown in Fig. 1(c), N-Gr presents the typical bands at 1578 and 1340 cm^{-1} attributed to G and D bands of graphene. The D band is originated from disordered sp^3 carbon that is caused by structural defects in graphene sheets, while the G band is ascribed to sp^2 carbon atoms vibration.[45] The intensity ratio (I_D/I_G) of the D band to G band is calculated as 0.84, aiming to judge the crystallizing structure of carbon materials and it demonstrated the comparatively high graphitization of N-Gr.[46] For PEDOS, the bands at 1430 cm^{-1} and 1480 cm^{-1} represent the symmetric $C_\alpha = C_\beta$ stretching. The bands at 1376 cm^{-1} and 1256 cm^{-1} are the $C_\beta = C_\beta$ and $C_\alpha = C_\alpha$ inter-ring stretching of selenophene rings. The band at 1072 cm^{-1} is assigned to the C–O–C deformation in the methylenedioxyphenol groups of PEDOS structure. For PEDOS/N-Gr, the bands at 1483 and 1425 cm^{-1} are ascribed to the symmetric $C_\alpha = C_\beta$ stretching of the selenophene rings in the PEDOS. The characteristic band for C=C in PEDOS (1525 cm^{-1}) has a slight shift to 1538 cm^{-1} in the composite due to the π–π interactions between PEDOS and N-Gr.[45,47] For PEDOT/N-Gr, the peaks at 1432 and 1514 cm^{-1} are corresponding to the symmetric $C_\alpha = C_\beta$ stretching of the thiophane rings in PEDOT. The characteristic band for C=C of PEDOT (1510 cm^{-1}) slightly shifts to 1514 cm^{-1} in the composites because of the π–π interactions between PEDOT and N-Gr. It is notable that after combined with polymer, the D and G bands from N-Gr are nearly invisible in PEDOS/N-Gr and PEDOT/N-Gr, due to the overlapping of bands by polymer at the same position. However, it can be observed that the bands of PEDOS/N-Gr shift to lower frequency compared with the pure PEDOS, which is not obvious in the PEDOT/N-Gr bands, indicating strong interaction between PEDOS and N-Gr than that of PEDOT and N-Gr.

Fig. 1(d) presents the UV-vis of PEDOS, PEDOT, N-Gr, PEDOS/N-Gr and PEDOT/N-Gr using *N*-methyl-2-pyrrolidone as solvent. The band of N-Gr appears at 320 nm that is associated with the transitive of C=C, and the broad bands at 455 to 500 nm originates from the n–π* transition in C=N.[48] In the case of PEDOS, there is a broad band at 488 nm, which implies the transitive n–π* in the polymer main chains. PEDOS/N-Gr displays characteristic broad absorption bands at 366 and 514 nm, which is ascribed to the π–π* and n–π* transition, respectively. It also indicated that the combination of N-Gr increases the conjugation degree of PEDOS, due to the large surface area from N-Gr. However, for PEDOT/N-Gr, the band for π–π* transition is located at 482 nm, while the band for π–π* transition of pure PEDOT is found at 505 nm, indicating that

the combination of N-Gr dose not increase the PEDOT conjugation degree. Therefore, it can be concluded that the interaction between N-Gr and PEDOS is stronger than that of PEDOT and N-Gr, and these results are well consistent with the Raman.

To further investigate the interaction between PEDOS and N-Gr, the chemical states of the carbon, selenium and nitrogen atoms are analysed by XPS and the corresponding regression coefficients are annotated in Fig. 2. Table S1 (ESI†) displays the elements content of the N-Gr, PEDOS, PEDOS/N-Gr from XPS analysis. Fig. 2(a)–(d) exhibits the XPS of N-Gr and PEDOS/N-Gr. The sharp peaks at 285, 56 and 401 eV in the wide-scan XPS (Fig. 2(a)) confirm the existence of C, Se and N atoms. As illustrated in Fig. 2(b), there are several peaks for N-Gr at 283.98, 285.88, 288.08, 289.88 and 291.58 eV, which belong to C–C, C–OH, C–N(C=O), C–C=O and O=C–O, indicating the existence of these functional correlation groups in N-Gr.[49] To compare the XPS data of PEDOS/N-Gr with PEDOS, an obvious reduction area for the C–Se combination intensity and an affective shift by 0.1 eV are observed, due to the strong interactions between N-Gr and PEDOS. The Se 3d spectra of PEDOS/N-Gr shows spin-split doublet peaks at 56.5 (Se $3d_3$) and 55.8 eV (Se $3d_5$) in Fig. 2(c). It can be seen in Fig. 2(d) that the combination configurations of the nitrogen atoms, and the inferior binding energy at 398.48 eV is attributed to pyridinic N and the one at 400.28 eV to pyrrolic N, owing to the pairs of π-electrons in the N-Gr. It is not only beneficial for the π-conjugated system, but also improves the electrical conductivity. The characteristic peak at 402.46 eV is specified to oxidized N and the positive shift (0.15 eV) due to the intensity of the C–Se, indicating that there is the strong interaction and incorporation between N-Gr and PEDOS composite.[50–52]

Morphology analysis

TEM image of the N-Gr displays a wrinkle layered structure (Fig. S2 (ESI†)), and the decorated wrinkles can be obviously discovered on the plane which is a representative character of few-layered graphenes.[53] Fig. 3 illustrates the SEM of N-Gr, PEDOS, PEDOT, PEDOS/N-Gr and PEDOT/N-Gr. As shown in Fig. 3(a), the N-Gr has a typical wrinkled wave and an ultrathin silk-like morphology of wrinkled graphene sheet structure, while PEDOS (Fig. 3(b)) displays a dense shape of small particles on the surface with high agglomeration. After the incorporation of N-Gr, the PEDOS/N-Gr (Fig. 3(c)) shows numerous interconnected PEDOS nanofilms on the N-Gr, and exhibits a very tough and irregular surface. This further indicates the strong electrostatic and π–π interactions between the EDOS molecules with N-Gr.[54] In addition, during the polymerization process, N-Gr and EDOS act as an electron acceptor and an electron donor, respectively. Therefore, nucleation sites for the polymer chain growth can be provided by large surface of N-Gr nanosheets and contribute to the uniform coating by PEDOS films. Fig. 3(d) displays a fibrous network-like morphology of PEDOT. According to the previous reports, under rapid initiated condition, the initial nano fibrous oligomers of EDOT can be occurred and play the role of soft template for the formation of nano fibrous structures. With the increase of reaction time, these nano fibrous oligomers are stacked to form a three-dimensional irregular fibrous network. It is interesting that the fibrous network-like morphology is present in PEDOT, while absent in the PEDOS which tends to form high agglomeration granules. This phenomenon can be understood that selenium atom has larger radius and is easier to polymerization compared with sulphur atom, which allows selenophene rings to hold more charges than the thiophene rings and favour to be activated at initiation process. Because the stronger interaction between PEDOS molecular chains than that of PEDOT, the initial nano fibrous oligomers of EDOS are stacked to from granular particles, and not three-dimensional irregular network. Fig. 3(e) shows that the PEDOT/N-Gr forms a nanofibrous when look closely, revealing that some of N-Gr are not covered with PEDOT. This means that the presence of N-Gr slightly affects the morphology of PEDOT in composite, and there is lower interaction between them.

To further investigate the elemental distribution of PEDOS and PEDOS/N-Gr, the elements such as carbon, oxygen, selenium and nitrogen are analysed by elemental mapping images (Fig. S3 (ESI†)). As depicted in Fig. S3(b) (ESI†), the C, O, Se and N atoms of PEDOS/N-Gr distribute uniformly on the

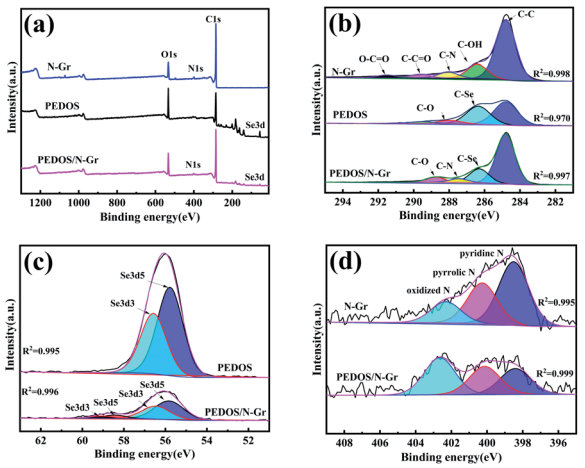

Fig. 2 (a) XPS full spectrum of PEDOS and PEDOS/N-Gr composites, (b) C 1s of PEDOS and PEDOS/N-Gr, (c) Se 3d of PEDOS and PEDOS/N-Gr, (d) N 1s of N-Gr, PEDOS and PEDOS/N-Gr.

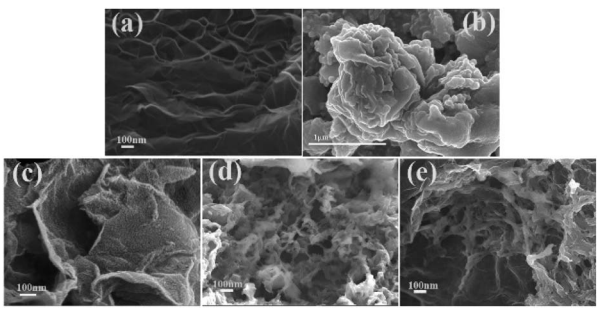

Fig. 3 SEM of (a) N-Gr, (b) PEDOS, (c) PEDOS/N-Gr, (d) PEDOT, and (e) PEDOT/N-G.

composite matrix. This further proves the results of morphological study, from which it is concluded that the surface of N-Gr can be uniformly coated by PEDOS. This uniform distribution of main elements increases the electrochemical active surface for oxidation of analytes and is beneficial to improve the sensitivity for determination of analyte molecules.

Electrocatalytic performance

To investigate the electrochemical behaviour of GCE electrodes that are modified by PEDOS/N-Gr, PEDOT/N-Gr composites and PEDOS, PEDOT polymers, the CV was conducted in the mixture solution of 5.0 mM $Fe(CN)_6^{3-/4-}$ and 0.1 M KCl at a stable scanning rate of 50 mV s^{-1}. Fig. 4 shows that there is a pairs of oxidation/reduction peaks of $[Fe(CN)_6]^{3-/4-}$ on bare GCE and modified GCE by all products. Furthermore, the peak-to-peak potential ($\Delta E_p = E_{anodic\ peak} - E_{cathodic\ peak}$) of composites (96 mV for PEDOS/N-Gr; 116 mV for PEDOT/N-Gr) is smaller than respective polymer (115 mV for PEDOS/GCE; 137 mV for PEDOT/GCE) (Table 1). This suggests that PEDOS/N-Gr/GCE has a superior electrochemical ability, which results from more electroactive sites and higher electron transfer ability on it.[55,56]

Optimization of experimental conditions

The DPV (Fig. S4a–d (ESI†)) performance of PEDOS/N-Gr modified GCE is conducted in 0.1 M PBS solution, to examine the effects of different pH values (pH = 3.0–9.0) on detecting the oxidation of 5 μM DA. It is found that pH values obviously influence the peak current of DA, and the optimal current response is observed at pH = 7. Therefore, the optimal pH value is used for the following test to obtain a highly sensitive detection of DA.

Determination of DA

In order to scientifically analyse the relationship between performance and structure, the detection of DA was investigated using DPV method. The electroactive performances of composite-modified electrodes were compared and evaluated. The effective electrode surface area was calculated through the Randle–Sevcik equation[57] (detailed calculations were depicted in the ESI†), giving the calculated surface area values for bare GCE, PEDOT/N-Gr/GCE and PEDOS/N-Gr/GCE as 0.132, 0.29 and 0.37 cm^2, respectively (Fig. 5).

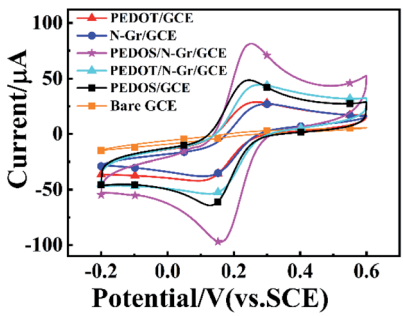

Fig. 4 CV of samples modified GCE in a 5.0 mM $Fe(CN)_6^{3-/4-}$/0.1 M KCl solvent.

Table 1 The peak potential (DEP) of modified GCEs

Modified GCE	$E_{anodic\ peak}$ (mV)	$E_{cathodic\ peak}$ (mV)	DEP (mV)
N-Gr	275	133	142
PEDOS	244	129	115
PEDOS/N-Gr	252	156	96
PEDOT	259	122	137
PEDOT/N-Gr	267	14	116

The results indicated that the effective electrode surface area of PEDOS/N-Gr/GCE was almost 3-fold higher than the bare GCE. Based on the effective electrode surface area, electrochemical sensitivities were as 28.9 μA μM^{-1} cm^{-2} for PEDOS/N-Gr/GCE and 7.93 μA μM^{-1} cm^{-2} for PEDOT/N-Gr/GCE. The limit of detection (LOD) and limit of quantification (LOQ) were calculated using the formulas of LOD = 3.0 S/N and LOQ = 10 S/N.[58] In that formula, S was the standard deviation of the intercept and N was the slope of the corresponding linear relationship of the tested samples. The LOD and LOQ values of PEDOS/N-Gr/GCE and PEDOT/N-Gr/GCE were calculated as 0.0066 μA, 0.02 μM and 0.018 μM, 0.056 μM for the detection of DA respectively. Detailed electrochemical characterizations reveals that the electrocatalytic activity is related to the structure of target biomolecules *via* the hydrogen bonding and π–π stacking between the DA and composite. To compared linear range and detection limit of this work with the previous reports on DA detection, different electrode sensor materials are illustrated in Table 2. It suggested that the PEDOT/N-Gr and PEDOS/N-Gr composites modified GCE for the DA detection exhibits

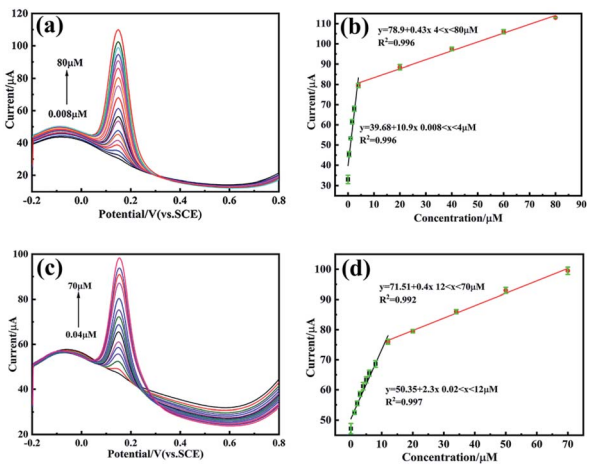

Fig. 5 (a)The DPV of PEDOS/N-Gr/GCE in a PBS solution (pH = 7.0) (DA: 0.008–80 μM), (b) the linear relationship between DPV current and concentration of DA for PEDOS/N-Gr/GCE (calibration curve error bars of PEDOS/N-Gr/GCE for three times), (c) the DPV of PEDOT/N-Gr/GCE in a PBS solution (pH = 7.0) (DA: 0.04–70 μM), (d) the linear relationship between DPV current and concentration of DA for PEDOT/N-Gr/GCE (calibration curve error bars of PEDOT/N-Gr/GCE for three times).

Table 2 The comparison of the electrochemical sensing properties to the different materials for DA detection[a]

Electrode	Technique	Linear range (μM)	LOD (μM)	Sensitive (μA μM^{-1} cm^{-2})	Ref.
NG/PEDOT/GCE	DPV	0.2–90	0.054	0.9	30
Co–N–C-800/RDE	CV	0.06–1200	0.04	979.6	60
MoS_2-PANI/rGO/GCE	DPV	5.0–500	0.70	—	61
PEDOT/GO/GCE	DPV	6.0–200	2	—	62
PANI-GO/GCE	DPV	2–18	0.5	7.36	29
PDEA/MWCNT/GO/GCE	DPV	0.06–4.2, 4.2–18.2	0.042	—	63
GPCP PMB-GR/CILE	DPV	0.5–1020	0.15	0.902	64
	DPV	0.02–800	0.0056	—	65
PEDOT/N-Gr/GCE	DPV	0.04–70	0.018	7.9	This work
PEDOS/N-Gr/GCE	DPV	0.008–80	0.0066	28.9	This work

[a] NG = nitrogen-doped graphene, GCE = glassy carbon electrode, PANI = polyaniline, rGO = reduced graphene oxide, RDE = rotation disk electrode, GO = graphene oxide, PDEA = poly(*tert*-butylacrylate)-*b*-(*N*,*N*-diethylacrylamide)-*b*-(*tert*-butyl acrylate) (*t*BA-PDEA-*t*BA), MWCNT = multi-walled carbon nanotubes, GPCP = reduced graphene oxide/poly(pyronine Y)/silver nanoparticle composite paper, PMB = poly(methylene blue), GR = functionalized graphene, CILE = carbon ionic liquid electrode.

a lower detection limit (0.04–70 μM and 0.008–80 μM). The mechanism for electrooxidation of DA can be seen from Scheme S2 (ESI†). DA is directly electrooxidized into dopamine-*o*-quinone (D-*o*-Q), and the electrochemical performance of DA redox couple was projected *via* the electron transfer–chemical reaction–electron transfer (ECE) mechanism.[59]

Interference study, stability and reproducibility of modified GCE

The interference study of PEDOS/N-Gr/GCE in 0.1 M PBS (pH = 7) solution is shown in Fig. 6. The UA, AA, SO_4^{2-}, NO_3^-, Na^+, Cl^- are chosen as the interfering substances in this work. After 5 μM DA was added, it can be seen that the current signals of UA and AA were slightly influenced and other interfering substances have no effect when successively injecting each of them up to 50 μM for PEDOS/N-Gr/GCE (Fig. 6) and (Fig. S5 (ESI†)), implying that this sensor has greater anti-interference ability. The stability of the PEDOS/N-Gr/GCE and PEDOT/N-Gr/GCE was investigated using DPV (Fig. S6(a) and (b) (ESI†)). The DPV response is collected on the one GCE for ten times in 0.1 M PBS solution (pH = 7) containing 5 μM DA. The values of RSD were about 1.56% and 1.24%, indicating that the PEDOS/N-Gr/GCE and PEDOT/N-Gr/GCE showed a high repeatability.

The reproducibility test was employed to evaluate the sensing ability of PEDOS/N-Gr/GCE in 0.1 M PBS solution (pH = 7.0) including 20 mM DA. After that, five mutual independent electrodes were used for the reproducibility test under optimal conditions. Fig. S7 (ESI†) showed the change in the peak current after the five parallel tests. The peak current of PEDOS/N-Gr/GCE slightly changes, and the RSD for DA detection is 1.026% and 1.746% for PEDOS/N-Gr/GCE and PEDOT/N-Gr/GCE, respectively.

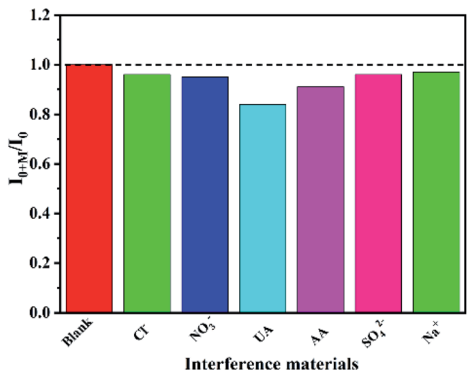

Fig. 6 Interference test of PEDOS/N-Gr/GCE by DPV measurement in 0.1 M PBS buffer solution.

Analysis of the real samples

To evaluate the practical application of PEDOS/N-Gr/GCE in real samples, electrochemical test of DA was performed in human serum and urine by a standard addition method. The human serum and urine were centrifuged, filtered and collected to obtain the clear liquid before detection. The samples were diluted 100 times with PBS solution (0.1 M, pH = 7), then the two concentration levels (10.0 and 30.0 μM) of DA were added into the samples to test the recovery before the electrochemical detection. The results are shown in Table 3, in which the PEDOS/N-Gr/GCE implies good recovery ranged from 95.40–100.14% for human serum and urine samples, suggesting that PEDOS/N-Gr/GEC is as an excellent electrochemical sensor for detecting DA in real samples.

Table 3 Detection of DA added in human serum and urine

	Human serum		Human urine	
Added (μM)	Found (μM)	Recovery (%)	Found (μM)	Recovery (%)
0	Not found	—	Not found	—
10	10.014	100.14	9.753	97.53
30	29.24	97.50	28.62	95.40

Conclusion

In this paper, the PEDOS/N-Gr composite was prepared for the electrochemical detection of DA by the DPV, and its structure and properties were compared with PEDOT/N-Gr prepared by the same method. The results indicated that N-Gr sheets were encapsulated by PEDOS, due to the π–π stacking between PEDOS and N-Gr. The structure and morphology analyses confirmed that the conjugation degree of the PEDOS/N-Gr was increased when compared with other samples. The electrochemical performance of PEDOS/N-Gr/GCE depicted a lower LOD value and a higher sensitivity than PEDOT/N-Gr/GCE, owing to that the Se atoms are more favourable to oxidative polymerization than S atoms. The lower band gap of polymer may cause the increase of electron transport rate *via* intermolecular Se–Se interaction in the PEDOS, which further enhances the oxidation ability of the composite to the detected molecular. Moreover, the combination of polymers and N-Gr could expose the more active sites for DA and increase the electrochemical sensitivity and stability. Detailed electrochemical characterizations revealed that the electrocatalytic activity was related to the structure of target biomolecules by hydrogen bonding and π–π stacking between the DA and PEDOS. The analysis results of actual samples showed that the composite of PEDOS/N-Gr has excellent recovery (95.40–100.14%) for human serum and urine samples. All these factors proved the high electrocatalytic activity of PEDOS/N-Gr modified GCE for the electrochemical detection of DA, suggesting that as-prepared composite was a promising material for electrochemical sensors in practical applications.

Ethical statement

The human serum and urine samples obtained from laboratory healthy classmates. All experiments were performed in accordance with the guidelines established by the National Institutes of Health. Experiments were approved by the ethics committee at Xinjiang University. Informed consents were obtained from human participants of this study.

Author contributions

Aygul Kadir: data curation, methodology, investigation, software, writing-original draft preparation, review& editing. Nurbiye Sawut: methodology, investigation. Yuzhu Che: review, investigation. Zulpikar Helil: language spelling, investigation. Hujun Zhang: investigation, software editing. Ruxangul Jamal: resources, project administration, methodology, editing. Tursun Abdiryim: conceptualization, validation, review & editing.

Conflicts of interest

The authors declare that there are no conflicts of interest.

Acknowledgements

We gratefully acknowledge the financial support from the National Natural Science Foundation of China (No. 52163020, No. 21764014).

Notes and references

1 X. Zhang, Y. C. Zhang and L. X. Ma, *Sens. Actuators, B*, 2016, **227**, 488–496.
2 A. Joshi, W. Schuhmann and T. C. Nagaiah, *Sens. Actuators, B*, 2016, **230**, 544–555.
3 M. Choudhary, R. Brink, D. Nandi, S. Siwal and K. Mallick, *J. Mater. Sci.*, 2017, **52**, 770–781.
4 I. Iftikhar, K. M. A. El-Nour and A. Brajter-Toth, *Electrochim. Acta*, 2017, **249**, 145–154.
5 L. Fraisse, M. C. Bonnet, J. P. De Farcy, C. Agut, D. Dersigny and A. Bayol, *Anal. Biochem.*, 2002, **309**, 173–179.
6 Y. Wang, L. Xiao and M. Cheng, *J. Chromatogr. A*, 2011, **1218**, 9115–9119.
7 J. Domínguez-álvarez, M. Mateos-Vivas, D. García-Gómez, E. Rodríguez-Gonzalo and R. Carabias-Martínez, *J. Chromatogr. A*, 2013, **1278**, 166–174.
8 Y. Yuan, S. Han, L. Hu, S. Parveen and G. Xu, *Electrochim. Acta*, 2012, **82**, 484–492.
9 S. Li, X. Li, J. Xu and X. Wei, *Talanta*, 2008, **75**, 32–37.
10 P. Nagaraja, R. A. Vasantha and K. R. Sunitha, *J. Pharm. Biomed. Anal.*, 2001, **25**, 417–424.
11 A. A. Abdelwahab and Y. B. Shim, *Sens. Actuators, B*, 2015, **221**, 659–665.
12 M. Ahn and J. Kim, *J. Electroanal. Chem.*, 2012, **683**, 75–79.
13 D. N. Oko, S. Garbarino, J. Zhang, Z. Xu, M. Chaker, D. Ma, D. Guay and A. C. Tavares, *Electrochim. Acta*, 2015, **159**, 174–183.
14 A. Malinauskas, R. Garjonyte, R. Mažeikiene and I. Jurevičiute, *Talanta*, 2004, **64**, 121–129.
15 A. C. Acta and M. Pravda, *Anal. Chim. Acta*, 2014, **431**, 239–247.
16 L. J. Sun, Z. Q. Pan, J. Xie, X. J. Liu, F. T. Sun, F. M. Song, N. Bao and H. Y. Gu, *J. Electroanal. Chem.*, 2013, **706**, 127–132.
17 M. Giannetto, G. Mori, F. Terzi, C. Zanardi and R. Seeber, *Electroanalysis*, 2011, **23**, 456–462.
18 L. Yang, S. Liu, Q. Zhang and F. Li, *Talanta*, 2012, **89**, 136–141.
19 X. Wang, Y. Shen, A. Xie, S. Li, Y. Cai, Y. Wang and H. Shu, *Biosens. Bioelectron.*, 2011, **26**, 3063–3067.
20 T. Qian, C. Yu, X. Zhou, S. Wu and J. Shen, *Sens. Actuators, B*, 2014, **193**, 759–763.
21 W. Zhang, R. Yuan, Y. Q. Chai, Y. Zhang and S. H. Chen, *Sens. Actuators, B*, 2012, **166–167**, 601–607.
22 C. Hou, H. Liu, D. Zhang, C. Yang and M. Zhang, *J. Alloys Compd.*, 2016, **666**, 178–184.
23 T. Kokulnathan and S. M. Chen, *ACS Sustainable Chem. Eng.*, 2019, **7**, 4136–4146.
24 S. Patra, E. Roy, A. Tiwari, R. Madhuri and P. K. Sharma, *Biosens. Bioelectron.*, 2017, **89**, 8–27.

25 J. Chen, Y. Han, X. Kong, X. Deng, H. J. Park, Y. Guo, S. Jin, Z. Qi, Z. Lee, Z. Qiao, R. S. Ruoff and H. Ji, *Angew. Chem., Int. Ed.*, 2016, **55**, 13822–13827.
26 L. Qin, R. Ding, H. Wang, J. Wu, C. Wang, C. Zhang, Y. Xu, L. Wang and B. Lv, *Nano Res.*, 2017, **10**, 305–319.
27 S. De Liberato, C. Ciuti, D. Auston, M. Nuss, S. Keiding, M. Van Exter, C. Fattinger, A. J. Taylor, C. Highstrete, M. Lee, R. D. Averitt, E. Smirnova, A. Azad, H. Chen, G. Scalari, M. I. Amanti, M. Beck and J. Faist, *Science*, 2012, **335**, 1326–1330.
28 D. C. Marcano, D. V. Kosynkin, J. M. Berlin, A. Sinitskii, Z. Sun, A. Slesarev, L. B. Alemany, W. Lu and J. M. Tour, *ACS Nano*, 2010, **4**, 4806–4814.
29 P. Manivel, M. Dhakshnamoorthy, A. Balamurugan, N. Ponpandian, D. Mangalaraj and C. Viswanathan, *RSC Adv.*, 2013, **3**, 14428–14437.
30 H. Teng, J. Song, G. Xu, F. Gao and X. Luo, *Electrochim. Acta*, 2020, **355**, 136772.
31 G. Fabregat, J. Osorio, A. Castedo, E. Armelin, J. J. Buendía, J. Llorca and C. Alemán, *Appl. Surf. Sci.*, 2017, **399**, 638–647.
32 Z. Liu, B. Lu, Y. Gao, T. Yang, R. Yue, J. Xu and L. Gao, *RSC Adv.*, 2016, **6**, 89157–89166.
33 A. Patra, M. Bendikov and S. Chand, *Acc. Chem. Res.*, 2014, **47**, 1465–1474.
34 A. Patra, Y. H. Wijsboom, S. S. Zade, M. Li, Y. Sheynin, G. Leitus and M. Bendikov, *J. Am. Chem. Soc.*, 2008, **130**, 6734–6736.
35 S. S. Zade and M. Bendikov, *Org. Lett.*, 2006, **8**, 5243–5246.
36 M. Li, A. Patra, Y. Sheynin and M. Bendikov, *Adv. Mater.*, 2009, **21**, 1707–1711.
37 M. Li, Y. Sheynin, A. Patra and M. Bendikov, *Chem. Mater.*, 2009, **21**, 2482–2488.
38 A. Patra and M. Bendikov, *J. Mater. Chem.*, 2010, **20**, 422–433.
39 J. W. Park, S. J. Park, O. S. Kwon, C. Lee, J. Jang, J. Jang, J. W. Park, S. J. Park, C. Lee and O. S. Kwon, *Chem. Mater.*, 2014, **26**, 2354–2360.
40 J. L. Pozzo, G. M. Clavier, M. Colomes and H. Bouas-Laurent, *Tetrahedron*, 1997, **53**, 6377–6390.
41 H. Liu, W. Zhou, X. Ma, S. Chen, S. Ming, K. Lin, B. Lu and J. Xu, *Electrochim. Acta*, 2016, **220**, 340–346.
42 Y. Lu, C. Kacica, S. Bansal, L. M. Santino, S. Acharya, J. Hu, C. Izima, K. Chrulski, Y. Diao, H. Wang, H. Yang, P. Biswas, J. Schaefer and J. M. D'Arcy, *ACS Appl. Mater. Interfaces*, 2019, **11**, 47320–47329.
43 B. Kim, J. Kim and E. Kim, *Macromolecules*, 2011, **44**, 8791–8797.
44 Y. Wei, L. Xu, Y. Tao, C. Yao, H. Xue and Y. Kong, *Ind. Eng. Chem. Res.*, 2016, **55**, 1912–1920.
45 Y. Shao, S. Zhang, M. H. Engelhard, G. Li, G. Shao, Y. Wang, J. Liu, I. A. Aksay and Y. Lin, *J. Mater. Chem.*, 2010, **20**, 7491–7496.
46 T. Zhou, Y. Zhou, R. Ma, Z. Zhou, G. Liu, Q. Liu, Y. Zhu and J. Wang, *Carbon*, 2017, **114**, 177–186.
47 J. Zhang and X. S. Zhao, *J. Phys. Chem. C*, 2012, **116**, 5420–5426.
48 X. Wang, Y. Ding, H. Lu, F. Chen, N. Zhang and M. Ma, *Chem. Eng. J.*, 2018, **347**, 754–762.
49 Z. H. Sheng, L. Shao, J. J. Chen, W. J. Bao, F. Bin Wang and X. H. Xia, *ACS Nano*, 2011, **5**, 4350–4358.
50 Y. Wang, S. Zhao, Y. Zhang, W. Chen, S. Yuan, Y. Zhou and Z. Huang, *Appl. Surf. Sci.*, 2019, **463**, 1–8.
51 J. Huang, P. Meng and X. Liu, *J. Alloys Compd.*, 2019, **805**, 654–662.
52 Z. Liu, J. Xu, R. Yue, T. Yang and L. Gao, *Electrochim. Acta*, 2016, **196**, 1–12.
53 Y. Wu, D. Yu, Y. Feng, L. Han, X. Liu, X. Zhao and X. Liu, *Chin. Chem. Lett.*, 2021, **9**, 56.
54 K. S. Choi, F. Liu, J. S. Choi and T. S. Seo, *Nanotechnology*, 2010, **26**, 12902–12908.
55 G. Zhao, Y. Yin, H. Wang, G. Liu and Z. Wang, *Electrochim. Acta*, 2016, **220**, 267–275.
56 L. Yang, N. Huang, Q. Lu, M. Liu, H. Li, Y. Zhang and S. Yao, *Anal. Chim. Acta*, 2016, **903**, 69–80.
57 R. N. Goyal, V. K. Gupta and S. Chatterjee, *Sens. Actuators, B*, 2010, **149**, 252–258.
58 H. Ibrahim and Y. Temerk, *Microchim. Acta*, 2020, **10**, 579.
59 J. Zhao, W. Zhang, P. Sherrell, J. M. Razal, X. Huang, A. I. Minett and J. Chen, *ACS Appl. Mater. Interfaces*, 2012, **4**, 44–48.
60 Y. Shu, Z. Li, Y. Yang, J. Tan, Z. Liu, Y. Shi, C. Ye and Q. Gao, *ACS Appl. Nano Mater.*, 2021, **4**, 7954–7962.
61 S. Li, Y. Ma, Y. Liu, G. Xin, M. Wang, Z. Zhang and Z. Liu, *RSC Adv.*, 2019, **9**, 2997–3003.
62 D. Li, M. Liu, Y. Zhan, Q. Su, Y. Zhang and D. Zhang, *Microchim. Acta*, 2020, **187**, 94–103.
63 P. Zhao, C. Chen, M. Ni, L. Peng, C. Li, Y. Xie and J. Fei, *Microchim. Acta*, 2019, **186**, 1–9.
64 K. D. Kıranşan, E. Topçu and M. Alanyalıoğlu, *J. Appl. Polym. Sci.*, 2017, **134**, 1–10.
65 W. Sun, Y. Wang, Y. Zhang, X. Ju, G. Li and Z. Sun, *Anal. Chim. Acta*, 2012, **751**, 59–65.